ACS Partner Journal

Journal of the American Society for Mass Spectrometry

pubs.acs.org/jasms

Research Article

# Probing Polyester Branching by Hybrid Trapped Ion-Mobility Spectrometry–Tandem Mass Spectrometry

Robert L. C. Voeten, Bram van de Put, Jan Jordens, Ynze Mengerink, Ron A. H. Peters, Rob Haselberg,* and Govert W. Somsen

Cite This: *J. Am. Soc. Mass Spectrom.* 2021, 32, 1498–1507

Read Online

ACCESS | Metrics & More | Article Recommendations | Supporting Information

**ABSTRACT:** Trapped ion-mobility spectrometry combined with quadrupole time-of-flight mass spectrometry (TIMS-QTOFMS) was evaluated as a tool for resolving linear and branched isomeric polyester oligomers. Solutions of polyester samples were infused directly into the ion source employing electrospray ionization (ESI). TIMS-MS provides both mobility and $m/z$ data on the formed ions, allowing construction of extracted-ion mobilograms (EIMs). EIMs of polyester molecules showed multimodal patterns, indicating conformational differences among isomers. Subsequent TIMS-MS/MS experiments indicated mobility differences to be caused by (degree of) branching. These assignments were supported by liquid chromatography-TIMS-MS/MS analysis, confirming that direct TIMS-MS provided fast (500 ms/scan) distinction between linear and branched small oligomers. Observing larger oligomers (up to 3000 Da) using TIMS required additional molecular charging to ensure ion entrapment within the mobility window. Molecular supercharging was achieved using *m*-nitrobenzyl alcohol (NBA). The additional charges on the oligomer structures enhanced mobility separation of isomeric species but also added to the complexity of the obtained fragmentation mass spectra. This complexity could be partly reduced by post-TIMS analyte-decharging applying collision-induced dissociation (CID) prior to Q1 with subsequent isolation of the singly charged ions for further fragmentation. The as-obtained EIM profiles were still quite complex as larger molecules possess more possible structural isomers. Nevertheless, distinguishing between linear and symmetrically branched oligomers was possible based on measured differences in collisional cross sections (CCSs). The established TIMS-QTOFMS approach reliably allows branching information on isomeric polyester molecules up to 3000 Da to be obtained in less than 1 min analysis time.

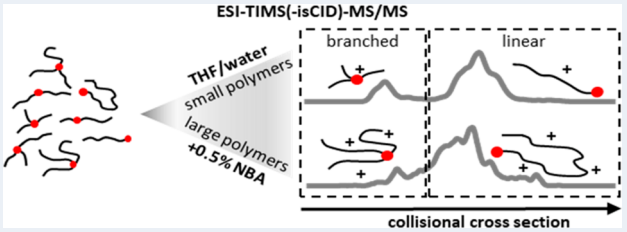


**KEYWORDS:** *polyesters, trapped ion-mobility spectrometry, TIMS, IMS-MS, high-resolution mass spectrometry, branching, polymer supercharging*

## INTRODUCTION

The ever-expanding fields of application for synthetic polymers not only derive from the introduction of new chemistries but also from subtle manipulation of polymer structures. Alterations on the molecular level can result in significantly different solid-state properties[1−4] and, thus, also in the characteristics of the produced material, defining its potential application field.[5] Polymer branching with short (~10 carbon units) or long side chains (>300 carbon units) is an essential property as it strongly affects crystallization behavior as well as rheological, flow, and mechanical properties.[6] Determination of the type, degree of branching (DB), and the distribution is therefore an important aspect for polymer production. Several techniques have so far been used for investigating branching,[7−11] including one- and two-dimensional $^{1}$H and $^{13}$C nuclear magnetic resonance spectroscopy (NMR),[7,12−17] capillary electrophoresis (CE),[18,19] size exclusion chromatography (SEC) with multiangle light scattering, differential viscometry, or dynamic light scattering, and differential refractometry detectors. Also differential scanning calorimetry (DSC),[20,21] matrix assisted laser desorption ionization (MALDI),[7,22] and electrospray ionization (ESI) mass spectrometry (MS)[7,10] are often applied.

SEC is the most used technique to determine the molecular weight distribution ($M_w$)[12,23] of polymers, but can also provide insights in the overall DB. Branched molecules exhibit reduced hydrodynamic volumes ($V_H$) relative to their linear counterparts of identical molar mass and elute later in SEC.[24] However, at a given elution volume often molecular weight dispersity and topological heterogeneity resulting from variation in $M_w$ and chain architecture results in broad nonresolved peaks.[8,12,25] Furthermore, dispersity often is overestimated and linear analogues (as references) are not

Received: February 24, 2021
Revised: April 28, 2021
Accepted: May 4, 2021
Published: May 14, 2021

always available, which is required to distinguish branched polymers.[12,26,27] CE can be employed to separate linear from branched chains in concordance with their electrophoretic mobility as they differ in $V_H$ and thus charge-to-size/shape ratio.[18,28] However, CE evidently only applies to charged polymers.[14] NMR is the only technique capable of determining the average DB quantitatively as shown for poly(acrylic acid)[29] and poly(alkyl acid).[30] However, NMR generally suffers from limited sensitivity concerning differentiating short-chain branching (as the concentration is low) and long-chain branches of various lengths (chains up to 300 carbon units are typically pooled together).[11] Therefore, NMR is most useful for polymers containing high levels of short-chain branching. Moreover, conventional carbon-NMR experiments can be time-consuming.[31] Nevertheless, the total number of branch sites is determinable based on the quaternary carbon-atoms that represent branching points.[32]

To date, one-dimensional analytics capable of separating molecules in accordance with both molar mass and the number of branches is not available.[24,26] Two-dimensional separation has shown potential toward determining the overall DB of polyesters (PES) in an offline as well as online fashion.[33−36] In particular, liquid phase separation in combination with high resolution MS (HR-MS) often provides complementary and corroborative results with which polymer identification can be easily realized. However, differentiation of coeluting isomeric architectures is not possible as these exhibit the same mass.

Recently, ion-mobility spectrometry (IMS), a gas phase mobility-based separation technique, has gained increasing attention in the area of molecular characterization, especially in combination with high-resolution (HR) MS. The mobility of a molecule is dependent on its mass, size, shape, and charge. Differences in molecular composition and structure, such as branching, may result in different molecular sizes and conformations and, in turn, may enable ion-mobility separation.[37] A recent IMS technology development is the trapped ion-mobility spectrometer (TIMS) introduced by Park et al. and commercialized by Bruker Daltonics (timsTOF). An extensive description of TIMS can be found elsewhere.[38,39] Briefly, a direct current (DC) electric field gradient is applied to hold ions stationary against a constant flow of drift gas. Ions are eluted from the TIMS analyzer by reducing the electric field strength over time, yielding ion-mobility-based separations. The TIMS instrument operates in a low electric field, thus preventing ion heating and fragmentation in the ion funnel.[40] Furthermore, it utilizes a dual-funnel so that accumulation of analytes can be performed parallel to the separation.[38] This allows for duty cycles up to 100%. The analytes are pushed into the funnels by the drift gas, which allows for small physical dimensions of the IMS cell while preserving, or even enhancing, analytical performance. In TIMS, an electric field gradient stagnates the analyte ions axially when their steady state drift velocity $v_d$ exactly counterbalances the drift gas velocity.[41] The stationary position of the "trapped" ion depends on their exhibited mobility that is often presented in its reduced form ($K_0$), i.e., normalized with respect to pressure and temperature. Mobilities can be converted to analyte collisional-cross sections (CCS; Ω), using the Mason−Schamps equation,[42] where $q$ is ion charge, $\mu$ is the reduced mass of ion and drift gas molecule, $k_b$ is the Boltzmann constant, and $T$ is temperature:

$$\Omega = \frac{3q}{16}\frac{1}{K_0}\sqrt{\frac{2\pi}{\mu k_b T}} \quad (1)$$

IMS-MS analysis on polymer systems has been performed earlier.[38,39,43−48] For instance, Foley et al. showed that IMS can separate linear from $n$-armed star-shaped poly(ethylene glycol)-based polymers (PEG) as their gas-phase compactness varies.[46] More recently, Austin et al. separated varying star-branched PEG architectures by utilizing multiply charged species.[49] With an increase in charge, the separation performance is typically enhanced as was previously shown by Morsa et al.[44] for linear, 4-arm, 6-arm, and 8-arm star polymers. Reports on IMS separation of isomeric polymer systems exhibiting small molecular or architectural differences, such as single unit variances, are scarce.

The aim of this study was to investigate the potential of TIMS-MS for the separation of isomeric PES. In particular its capability to resolve small polymer architectural differences and determination of the branching-point location. This was first realized for low molecular weight PES (500−1400 Da) as higher molecular weight analytes were not efficiently trapped within the available mobility range. To overcome limitations of observing larger structures (up to 3000 Da), polymer supercharging was attempted to ensure increase of analyte mobility. In order to extract valuable information from the highly charged structures, postmobility decharging was studied. This appeared imperative to reduce the complexity of the MS/MS data of the larger multiply charged ions.

## MATERIALS AND METHODS

Materials; nonstabilized tetrahydrofuran (THF >99.9%), sodium iodide (NaI >99.5%), *meta*-nitrobenzyl alcohol (*m*-NBA 98%), sulfolane (99%), propylene carbonate (PC 99.7%), formic acid (FA; MS-grade), acetonitrile (ACN; MS-grade), and isopropyl alcohol (IPA; MS-grade) were purchased from Sigma (The Netherlands). Water was of milli-Q grade (18.2 MΩ cm; Merck Millipore, MA, US). The PES consisted of various chemistries based on propylene glycol (PG), terephthalic acid (TPA), and/or trimethylolpropane (TMP) and were kindly provided by DSM Resins & Functional Materials (Waalwijk/Zwolle, The Netherlands). As PG was added in excess, the PES predominantly were alcohol terminated structures (see Figure 1A). Branched species were formed in the presence of trimethylolpropane (TMP) (Figure 1B). The branching point depends on the location of TMP incorporation.

The studied PES samples are listed in Table 1 together with the hydroxyl (OH) and acid value (AV) determined with $^{31}$P NMR. These values confirmed that the majority of the polymer chains are alcohol terminated. The number-average molecular mass and functionality values are also determined, which respectively represent the expected chain sizes and degree of branching. $^{1}$H NMR and $^{13}$C NMR experiments confirmed the overall composition of all samples, and these details are provided in the Supporting Information (SI).

Sample preparation stock solutions of 1.0 mg/mL were prepared and further diluted to 0.2 mg/mL, both in nonstabilized THF. Aliquots of the diluted solutions (100 μL) were further mixed with 400 μL THF, 490 μL water, and 10 μL 100 mM NaI in water yielding 20 μg/mL of polymer. NaI is added to promote formation of sodium adducts during electrospray ionization of the oligomers. Polymer supercharging was studied by adding pure *m*-NBA (l) to the sample


https://doi.org/10.1021/jasms.1c00071
J. Am. Soc. Mass Spectrom. 2021, 32, 1498−1507

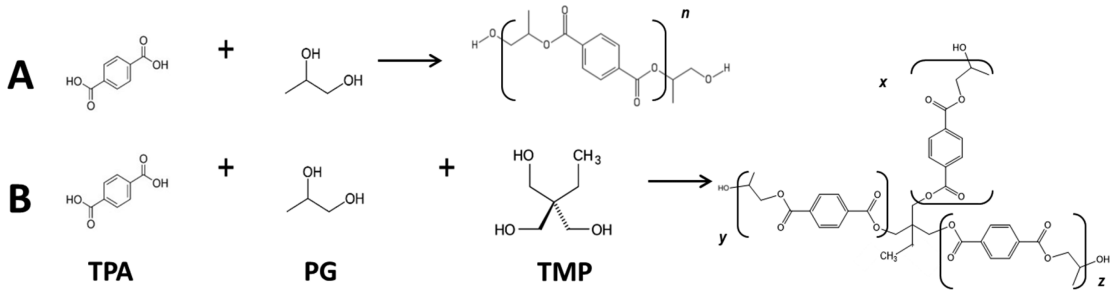


**Figure 1.** Polycondensation reaction of TPA and PG (A; top) and of TPA and PG in the presence of TMP (B; bottom). Here, $n \geq 1$ and $x \geq 1$, and $y, z \geq 0$.

solution to a final concentration of 0−1 vol%. For LC analysis, solutions of 1.0 mg/mL in THF/water/NaI (50/49/1 v/v/v) were prepared. All samples were passed through a 0.45 $\mu$m filter before analysis.

**Table 1. Studied PES Samples and Their Characteristics**

| sample | OH[a] | AV[a] | Mn[b] | F[b] |
|---|---|---|---|---|
| 1 | 45.2 | 1.9 | 2385 | 2.00 |
| 2 | 83.2 | 2.0 | 1848 | 2.84 |

[a]OH, hydroxyl value; AV, acid value. OH and AV were determined by $^{31}$P NMR. [b]$M_n$, calculated number average molecular mass; F, calculated functionality value. F is the average number of end groups per molecule. $F > 2$ indicates presence of branched structures.

TIMS-QTOFMS IMS-MS analysis was performed with a timsTOF instrument (Bruker Daltonics, Bremen, Germany) equipped with an ESI source. The instrument combines TIMS with high resolution quadrupole time-of-flight (qTOF)-MS. Data processing was performed using the DataAnalysis software version 5.1. The instrument was calibrated regarding mass and mobility daily or upon alteration of the instrumental settings, using MMI-TOF Tune Mix (Agilent Technologies, Waldbronn, Germany). Postanalysis calibration was also performed, to compensate for intermeasurement variation and to allow for semiautomated data processing. Taking into account a polycondensation reaction accompanied by the loss of water related to the extent of the reaction, the theoretical mass can be calculated per degree of polymerization. Subsequently, the formation of for instance sodium adducts upon ESI can be considered to attain the theoretical $m/z$ value.

The polymer solutions were directly infused (DI) into the ion source at a flow rate of 3 $\mu$L/min. Data was collected and averaged over a 1 min period. The ESI capillary voltage was 6000 V, the end plate offset 2000 V, the nebulizer pressure 0.3 bar, and the flow and temperature of the dry gas (nitrogen) 3.0 L/min and 200 °C, respectively. Unless otherwise stated, the measured ion mobility ($1/K_0$) range was 0.65−1.90 Vs/cm$^2$ using a 500 ms ramp (analyzer 2; Figure S1). The duty cycle was set to 100%, and the end of the mobility accumulation range is set to 2.00 Vs/cm$^2$ (analyzer 1; Figure S1). The so-called "D" parameters were optimized for the PES samples. These parameters are the potentials applied between particular regions in the TIMS analyzer, as shown in Figure S1, and affect the ion transmission efficiency and the dynamic mobility range in TIMS. The values were as follows for D1−6: 20, 0, 100, 200, 0, and 100 V, respectively.

MS/MS was used for structural elucidation of PES ions. The quadrupole was set to isolate predefined $m/z$ values ±2 $m/z$. The fragmentation energies were optimized for each particular $m/z$ of PES ions.

LC separation of PES samples was carried out using an Ultimate 3000 rapid separation UHPLC instrument (Thermo Scientific, MA, US) equipped with a dual pump, autosampler, column oven, and a diode array detector-ultraviolet detector set at 250 nm. A 2.1 × 150 mm Acquity C18 bridged ethylene hybrid (BEH, Waters) column with 1.7 $\mu$m particles was used. The mobile phase solvents consisted of (A) 0.1% formic acid in water and (B) ACN/IPA (70/30, v/v). The linear gradient was 25% B to 100% B in 35 min, kept at 100% B for 4 min, returning to 25% B in 0.1 min, and an equilibration at 25% B for 3 min. A 5 $\mu$L injection volume and a 0.3 mL/min flow were used. LC-TIMS-MS was performed with IMS off and IMS on. The timsTOF settings are as described in the previous section except nebulizer pressure (1.4 bar), dry gas flow (9.0 L/min), and source temperature (240 °C).

## RESULTS AND DISCUSSION

**DI-ESI-MS.** Figure 2 shows mass spectra of PES oligomers synthesized in the absence (sample 1, Table 1) and presence of TMP (sample 2, Table 1). PES oligomers predominantly yield sodium adducts, allowing assignment of their overall composition based on accurate mass after subtracting the mass of the sodium ion. Increments of 206 $m/z$ reflect repeating [TPA-PG] units and were annotated by an asterisk (*) in Figure 2. The signals at $m/z$ 511 and 569 were assigned

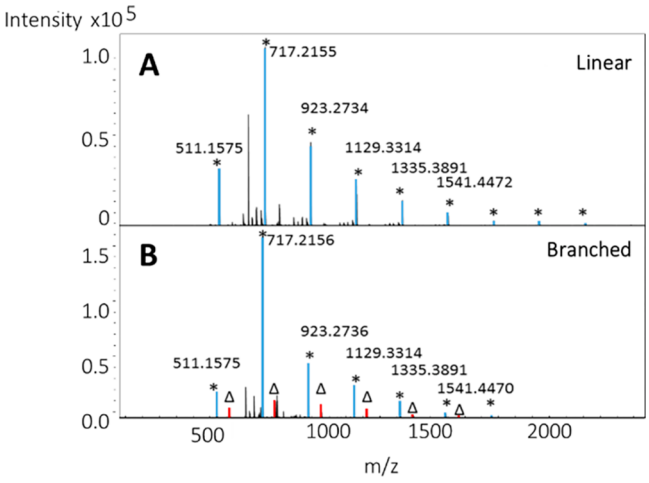


**Figure 2.** Mass spectra obtained during DI-ESI-MS of PES samples 1 (A) and 2 (B). Signals from $[(\text{TPA-PG})_n\text{-PG} + \text{Na}]^+$ ions (blue) are annotated by an asterisk and signals from $[(\text{TPA-PG})_n\text{-TMP} + \text{Na}]^+$ ions (red) are annotated by a delta.



https://doi.org/10.1021/jasms.1c00071
J. Am. Soc. Mass Spectrom. 2021, 32, 1498−1507

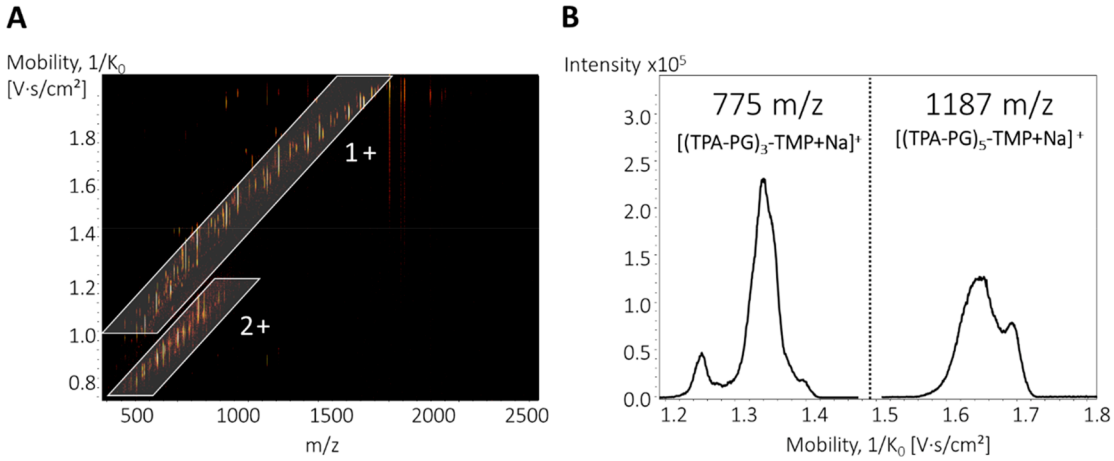


**Figure 3.** DI-ESI-TIMS-MS of PES oligomers. Heat map of sample 2 (A; 1+ and 2+ indicate charge of ions) and extracted-ion mobilograms (B) for $m/z$ 775 and 1187 as observed for sample 2.

to the smallest observed structures regarding linear and branched structures consisting of respectively $[(TPA\text{-}PG)_2\text{-}PG + Na]^+$ and $[(TPA\text{-}PG)_2\text{-}TMP + Na]^+$. Predominantly alcohol-terminated oligomers were observed; furthermore a limited number of monoacid functional oligomers (i.e., containing one alcohol (PG) and one acid end-group (TPA)), a very low number of acid-terminated oligomers, and no cyclic oligomers were detected. Distinction of TMP-incorporated and linear structures could be made based on the mass difference of 58 Da between PG and TMP (i.e., linear $[(TPA\text{-}PG)_n\text{-}PG]$ vs branched $[(TPA\text{-}PG)_n\text{-}TMP]$ molecules). TMP containing oligomers are annotated by a delta (Δ) in Figure 2. The TMP branching unit can be present at various locations within the oligomer structures, of which the occurrence and branching extent exhibit a particular probability. Resolving the resulting isomers with TMP at different positions is not possible by MS. As these isomers show a similar fragmentation behavior in collision-induced dissociation (CID), their reliable distinction by direct tandem MS is also not feasible. Resolution of the TMP-containing isomers requires separation prior to MS detection. For this we studied the potential of TIMS.

**DI-ESI-TIMS-MS.** The PES solutions were analyzed by DI-ESI-TIMS-MS, obtaining high-resolution mass spectra for each oligomer leaving the TIMS analyzer. The resulting array of mobility and $m/z$ data can be presented in a heat map as shown for sample 2 in Figure 3A. It clearly shows that the d.p. (degree of polymerization, i.e., the number of monomeric units) of the oligomer ions is inversely proportional to their mobility (upper trend indicated). A lower trend of signals in the heat map reveals doubly charged oligomer species, which consequently have a higher mobility (i.e., lower $1/K_0$) that also decreases with size (i.e., higher $1/K_0$). Interestingly, each oligomer ion observed at a specific $m/z$ value shows a mobility distribution (non-Gaussian) across a certain range. For each $m/z$, an extracted-ion mobilogram (EIM) can be constructed by averaging the data across an 1 min time span. Figure 3B shows the EIMs for $m/z$ 775 and 1187, which correspond to $[(TPA\text{-}PG)_3\text{-}TMP + Na]^+$ and $[(TPA\text{-}PG)_5\text{-}TMP + Na]^+$, respectively. The EIMs show a multimodal distribution, indicating the presence of isomeric species which significantly differ in ion mobility (RSD of CCS values 0.1−0.7% with an average of 0.3%; See Figure S2 and Table S1). The observed ion-mobility distribution might relate to the specific TMP location within the structure and to whether TMP has led to branching as visualized in Figure 4. In order to elucidate the actual structure of the PES isomers with different ion mobility, TIMS was combined with tandem MS.

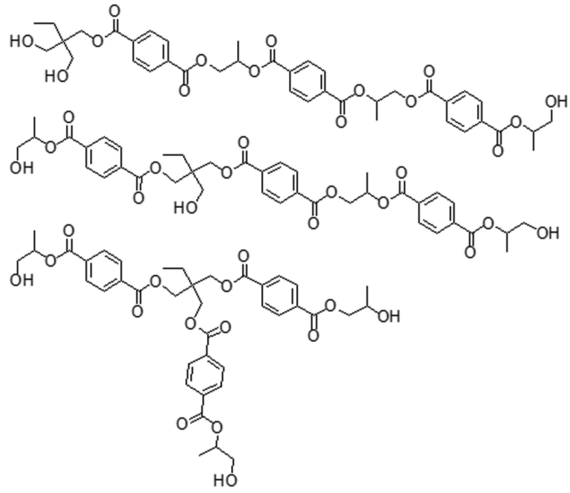

**Figure 4.** Structural isomers of [(TPA-PG)3-TMP] (d.p. = 7) indicating that TMP potentially can either be located at the end of the chain (top), in the chain without causing branching (middle), or in the chain causing branching (bottom).

**DI-ESI-TIMS-MS/MS.** To permit efficient MS/MS of the PES oligomer ions with $m/z$ 775, the funnel voltages were adjusted so that the measured $1/K_0$ range was between 1.15 and 1.40 Vs/cm$^2$, which is scanned with a rate of 500 ms. This time is adequate for MS/MS experiments. MS/MS results obtained using collision energies of 40 and 50 eV on the $m/z$ 775 ions observed in sample 2 are shown in Figure S3 top and bottom, respectively. These are average spectra obtained across the entire mobility window providing an overall dissociation pattern of the $m/z$ 775 ion. The most common fragmentation patterns of for the TMP containing PES is provided in Figure 5A. Assigned composition of ions observed during fragmentation of PES-oligomer ion with $m/z$ 775 are listed in Figure 5B and are formed via a charge remote 1,5-H rearrangement over the ester group as described by Wesdemiotis et al.[50] or via the charge migration fragmentation mechanism.[51]

The mass spectrum of the $m/z$ 775 ion (Figure 6A, top) with a mobility ($1/K_0$) of approximately 1.20−1.24 Vs/cm$^2$


https://doi.org/10.1021/jasms.1c00071
J. Am. Soc. Mass Spectrom. 2021, 32, 1498−1507

A

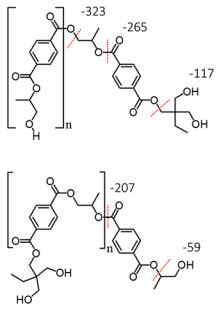


B

| m/z | Fragment* | |
|---|---|---|
| 207 | [PA+] | |
| 265 | [PAP+] | [TA+] |
| 323 | [PAT+] | |
| 355 | [APA+] | |
| 413 | [PAPA+] | |
| 471 | [PAPAP+] | [TAPA+] |
| 529 | [PAPAT+] | |
| 659 | $[ATAPA+Na]^+$ | $[PAPAPA+Na]^+$ |
| 717 | $[ATAPAP+Na]^+$ | |
| 775 | $[TAPAPAP+Na]^+$ | |

**Figure 5.** Most common fragmentation patterns for the TMP containing PES (A) and overall composition assignment of ions observed during fragmentation of PES-oligomer ion with $m/z$ 775 from sample 2 analyzed by DI-ESI-TIMS-MS/MS (B). Legend: P, propylene glycol; A, terephthalic acid; T, trimethylolpropane.

(Figure 6B, red) shows hardly any fragmentation and merely the precursor ion. Minor fragments are observed at $m/z$ 717 and 529, which could be assigned to the loss of a PG unit and a [TPA-PG] unit, respectively. These findings suggest that the top spectrum corresponds to a structure that contains TMP in the backbone of the polymer. The middle and bottom mass spectra (Figure 6A), corresponding to ions with a mobility of 1.25−1.30 Vs/cm$^2$ (Figure 6B, blue) and 1.30−1.35 Vs/cm$^2$ (Figure 6B, green), respectively, show similar fragment $m/z$ values. However, the intensities of $m/z$ 323 and 659 ions differ with respect to the parent peak $m/z$ 775 when comparing the middle and bottom mass spectra (e.g., $m/z$ 323:775 ratio is 1:8 (blue) and 1:2 (green)). This can be related to the probability with which particular fragments are formed. As ion-mobility separation takes place prior to ion fragmentation, EIMs of the product ions can be constructed. The resulting EIM profile can subsequently be compared to the parent-ion mobilograms. Figure 6B shows the EIMs constructed from the TIMS-MS/MS data obtained for the $m/z$ 775 ion with the trace for the parent ion (top), and the EIMs for the fragment ions at $m/z$ 323 (middle) and $m/z$ 659 (bottom). The latter two correspond to $[(TPA\text{-}PG)_1\text{-}TMP + Na]^+$ and a PES ion that lost two PG units or a single TMP unit, respectively. Three mobility regions as defined above (red, green, and blue) are indicated in the EIM traces. The parent-ion and $m/z$ 323 product-ion EIMs both show distributions between 1.25 and 1.35 $1/K_0$, whereas the parent EIM also shows a distribution between 1.20 and 1.25 $1/K_0$. From this it can be deduced that these higher mobility (i.e., lower $1/K_0$) species cannot exhibit an $m/z$ 323 fragment (assigned to the $[(TPA\text{-}PG)_1\text{-}TMP + Na]^+$ ion). To form this specific fragment from a branched structure requires a double $(TPA\text{-}PG)_1$ scission which is improbable. This finding supports the preliminary assignment above. Notably, the results imply that the branched structure has a smaller CCS (because larger $K_0$) and thus has a more compact conformation than the linear isomers.

The bottom EIM shows the $m/z$ 659 profile which has signals across the entire mobility range when compared to the parent EIM. Therefore, this profile cannot be used to identify a structurally unique fragment. However, the relative intensities per mobility region differ. This implies that the fragment is more likely to occur for the lower mobility structure (higher $1/K_0$; green area) as the intensity there is higher. The ion with $m/z$ 659 corresponds to the loss of either two PG units or one TMP unit, and it is reasonable to assume that dissociating one TMP end-group unit is more likely than simultaneously dissociating two PG units at opposite sides of the molecule. This would imply that the most intense mobility band corresponds to a structure that contains a TMP end-group (green area). In turn, the blue area corresponds to the structure where the TMP resides in the middle of the chain but does not constitute a branch site.

**LC(-UV)-TIMS-MS(/MS).** In order to support the structural assignment by DI-ESI-TIMS-MS/MS, sample 2 (branched PES) was also analyzed by LC-ESI-TIMS-MS. The attained base peak chromatogram is shown in Figure S4A. The most intense peaks observed at 9.5, 15.0, 17.5, 21.0, and 23.0 min correspond to $[(TPA\text{-}PG)_2\text{-}PG]$ up to $[(TPA\text{-}PG)_6\text{-}PG]$ oligomers, respectively. Multiple minor peaks are observed, e.g. six peaks appeared between 12 to 14 min. The extracted-ion chromatogram (EIC) of $m/z$ 775 (inset Figure S4A) shows that RPLC separates isomeric species.

Peaks 1, 2, and 3 exhibit ion-mobility values ($1/K_0$ 1.20−1.24 Vs/m$^2$; CCS of about 250 Å$^2$) that are similar to values previously found for the branched structures by DI-ESI-TIMS-MS (see Figure S4B). Subsequent LC-TIMS-MS/MS analysis revealed similar fragmentation spectra as for DI-ESI-TIMS-MS/MS. Indeed, it is plausible that the branched structures elute first in RPLC as the hydrophobic sites are more shielded by the hydrophilic end-groups. The reason that three peaks are

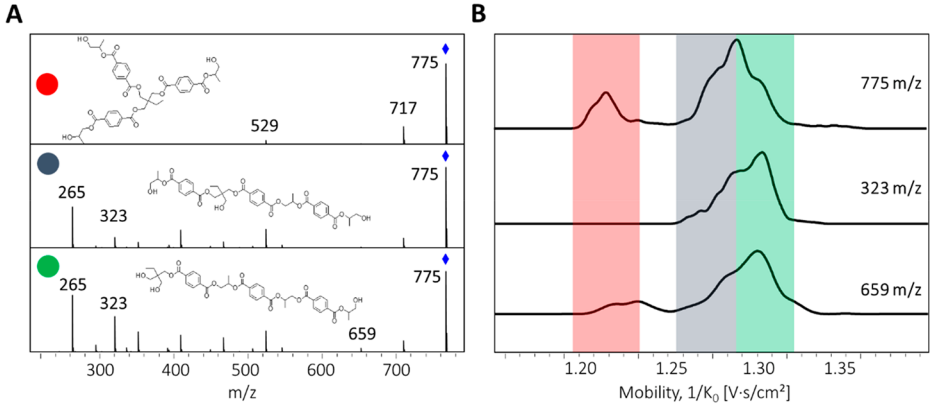


**Figure 6.** Mass spectra (A) and EIMs (B) for the $[(TPA\text{-}PG)_3\text{-}TMP + Na]^+$ ions obtained during TIMS-MS/MS of sample 2. Precursor EIM trace (B; top), 323 $m/z$ EIM (B; middle), and 659 $m/z$ EIM trace (B; bottom). The red, blue, and green circle indicate the mobility regions of which the averaged mass spectra are presented (A).



https://doi.org/10.1021/jasms.1c00071
J. Am. Soc. Mass Spectrom. 2021, 32, 1498−1507

obtained with RPLC can be related to the methyl side-group at the chiral center of the PG unit. The position of the methyl group will be on either one of the PG backbone carbons, which results in positional isomers and stereoisomers. Peaks 4 and 5 show more retention indicating of relatively more hydrophobic species, as is expected for the linear oligomers, containing a TMP in the structure. The acquired IMS data reveal mobility values ($1/K_0$) between 1.25 and 1.35 (CCS of 260−270 Å$^2$). The EIM traces of peaks 4 and 5 exhibit multimodality, which align with the fact that the TMP can either be an end-group or positioned within the polymer backbone. As indicated earlier, these isomeric structures have a slightly different mobility. The tandem MS spectra observed for the LC peaks were similar to those obtained for the DI-ESI-TIMS-MS/MS experiments. Overall, the RPLC-ESI-TIMS-MS(/MS) results confirm the previous assignments of the linear and branched structures by direct TIMS. Notably, peaks 6, 7, and 8 exhibit similar mobility values across the range of the parent EIM. Furthermore, MS/MS on these features showed similar fragmentation patterns as the analytes of interest.

**TIMS-MS OF Larger Oligomers.** TIMS-MS/MS is capable of resolving relatively small linear and branched PES structures. However, as can be seen in the heat map (Figure 3A), larger singly charged ions with an $m/z$ above 2000 are not observed within the mobility window as they are not captured by the electric field gradient. Detection of larger species requires additional charging of the molecules in order to increase their ion mobility (lower $1/K_0$). Under the applied conditions, the ionization efficiency of the larger molecules was too low to create useful EIMs. Therefore, multiple charging of the larger PES molecules by means of supercharging was attempted. In protein analysis, compounds such as glycerol, sulfolane, dimethyl sulfoxide (DMSO), propylene carbonate (PC), and *m*-nitrobenzyl alcohol (NBA) have been used for supercharging.[52−54] We tested sulfolane, PC, and NBA for PES oligomer analysis by adding these separately in varying concentrations to the sample solutions. Sulfolane did not yield enhanced signal intensities in ESI-MS for multiply charged PES species, and PC even caused charge reduction of PES molecules, as was also observed previously for other hydrocarbon-based polymers.[55] In contrast, NBA led to signal intensity enhancement of multiply charged PES ions. NBA will be present at the droplet interface where it interferes with the ejection of $Na^+$ ions from the droplets during ESI. This leads to increased charge density within the droplet promoting adduction of $Na^+$ ions with the molecules. The cumulative relative intensities of the most prominent ions of PES oligomers with $n$ = 7−12 observed upon ESI-MS, were plotted per charge state as a function of the concentration of NBA (0.0−1.0 vol%; Figure S5). NBA caused a slight reduction in intensity for singly and doubly charged PES ions, but the signal intensity of the triply charged PES ions ($m/z$ 666−1147: $[(\text{TMP-PG})_{12-16}\text{-PG} + 3\text{Na}]^{3+}$ and $[(\text{TMP-PG})_{12-16}\text{-TMP} + 3\text{Na}]^{3+}$) increased up to an average factor of 12 when using 0.5% NBA.

Supercharging of the larger PES molecules did provide ion mobilities that were within the measurable window of the TIMS instrument, i.e. between 0.65 and 1.90 $1/K_0$ and also led to enhanced separation power which will be discussed later on. However, subsequent tandem MS analysis of the multiply charged analytes—in order to extract structural information—resulted in complicated fragmentation patterns, showing triply, doubly, and singly charged fragments making assignment near-impossible. In order to reduce the complexity of the fragment spectra, a postmobility CID (pmCID) approach was applied to achieve removal of adduct ions (i.e., decharging) *after* the ions left the IM analyzer and before they entered the quadrupole. That is, a small electric field is applied at the lens of the second funnel leading to sodium stripping. The triply charged PES ions ($[\text{M} + 3\text{Na}]^{3+}$) were first resolved by ion-mobility and subsequently pmCID was used to remove sodium adduct ions providing $[\text{M} + \text{Na}]^+$ and $[\text{M} + 2\text{Na}]^{2+}$ ions that were subjected to MS(/MS) analysis. As the adduct-ion removal takes place after IM separation, the EIMs constructed for $[\text{M} + 2\text{Na}]^{2+}$ and $[\text{M} + \text{Na}]^+$ contain information on the virtual $[\text{M} + 3\text{Na}]^{3+}$ EIM. $[\text{M} + \text{Na}]^+$ and $[\text{M} + 2\text{Na}]^{2+}$ ions already generated during ESI obviously will also appear in the EIM; however, they will not overlap with the bands related to the original $[\text{M} + 3\text{Na}]^{3+}$ ions due to differences in $1/K_0$ values. The $[\text{M} + 2\text{Na}]^{2+}$ ions were used to construct the parent ion EIMs, and the $[\text{M} + \text{Na}]^+$ ions obtained after pmCID were isolated and fragmented for structural assignment. To illustrate this procedure, the IM separation of $[(\text{TPA-PG})_{11}\text{-TMP} + 3\text{Na}]^{3+}$ isomers is shown in Figure S6. The ion with $m/z$ 823 corresponds to triply charged species. The parent-ion EIM is constructed based on the $m/z$ 1223 ion, i.e. the doubly charged species ($[(\text{TPA-PG})_{11}\text{-TMP} + 2\text{Na}]^{2+}$). Fragmentation is subsequently performed on the $m/z$ 2424 ion, i.e. the singly charged molecule ($[(\text{TPA-PG})_{11}\text{-TMP} + \text{Na}]^+$).

The number of possible structures increases drastically for longer chains, making it more difficult to reliably assign structures to the observed IM bands. Moreover, observed fragments, such as the previously mentioned ion with $m/z$ 323, are no longer uniquely indicative for branched structures as the branching point can be at any position within the chain. Still, the $m/z$ 323 fragment ion will indicate the IM band that corresponds to a chain where the TMP group is at the end or one repeating unit from the end of the chain i.e. $[(\text{TPA-PG})_n\text{-TMP}]$ or $[(\text{TPA-PG})_{n-1}\text{-TMP-TPA-PG}]$. The spectral interpretation is illustrated in Figure S6, which shows EIMs obtained when analyzing sample 2 by TIMS-pmCID-MS/MS. The EIM of the $m/z$ 323 fragment ion shows a single IM band corresponding to the 1.04 $1/K_0$ peak of the parent EIM. By subsequently comparing the fragment EIM of the $m/z$ 323 ion with the fragment EIM at $m/z$ 529, which is one single repeating unit larger, it is evident that the latter exhibits two peaks. The right peak is at the same position as the EIM of $m/z$ 323 implying that the TMP is still a (near-)end group. The left band of the $m/z$ 529 EIM does not overlap with the $m/z$ 323 traces which implies that the TMP-group is more centrally located, or the extent of branching is larger (illustrated in Figure S7). This interpretation scheme can be expanded by successively evaluating increments of single repeating units and comparing these to the traces of shorter fragments. Any emerging peak that is not in overlap with a previous trace will provide information on the structure of the oligomer corresponding to that band and will allow distinguishing the linear and symmetrically branched structures. When the TMP is more centrally located, it becomes more difficult to distinguish small-chain branched structures from the linear structures, as the respective peaks will start to overlap strongly. This is for example shown in Figure 7, where the parent EIMs of oligomers with d.p. 21−27 are provided (i.e., $[(\text{TPA-PG})_{10}\text{-TMP} + 3\text{Na}]^{3+}$ up to $[(\text{TPA-PG})_{13}\text{-TMP} + 3\text{Na}]^{3+}$). The symmetrically branched (red dot) and linear (green dots) oligomers can still be assigned. However, the signals in the



https://doi.org/10.1021/jasms.1c00071
J. Am. Soc. Mass Spectrom. 2021, 32, 1498−1507

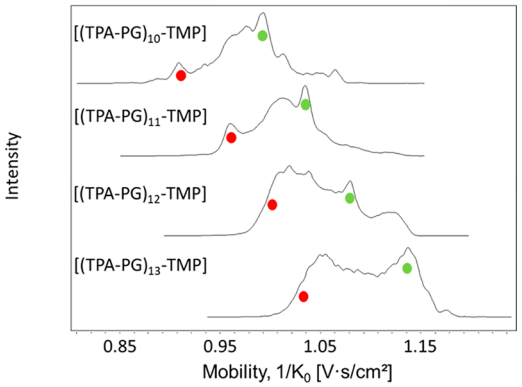


**Figure 7.** EIM traces of $[(\text{TPA-PG})_n\text{-TMP} + 3\text{Na}]^{3+}$ with $n$ = 10, 11, 12, or 13 from top to bottom. Indicated are the fully branched (red dot) and linear structures (green dot).

interstitial region are caused by other possible isomers, which include ions where the TMP is located more centrally and where the structure contains short-chain branches. Furthermore, the position of the sodium ions on the PES chains may also affect the CCS leading to wider distributions. Indeed, when the polymer sample solution was analyzed in the presence of the trivalent metal ion lanthanum, the peak widths of the EIMs of $[(\text{TPA-PG})_{13}\text{-TMP} + \text{La}]^{3+}$ was significantly more narrow (up to 4 fold) than the peak width of $[(\text{TPA-PG})_{13}\text{-TMP} + 3\text{Na}]^{3+}$. Clearly, the sodium ion location on the polymer chain influences the obtained CCS of the adduct ions complicating identification. The fragment EIM approach provides useful structural insights; however, its span is limited by the sheer number of possible oligomer structures, and corresponding similarity of their ion mobility values for which the current IM resolution is not sufficient.

As briefly mentioned, another benefit of multiple charging is the higher resolving power that is accompanied with IMS-MS analysis. It has been shown for linear and $n$-armed star-polymers that better isomer separation can be achieved when ions are multiply charged.[44] Molecular charging promotes electrostatic elongation of the polymer chains and therefore can improve resolution by IMS. This is evaluated in the current study for sample 2 by TIMS-pmCID-MS/MS employing the described approach for higher charged ions. EIMs of all perceived $m/z$ values were converted to CCS distributions. Subsequently, the CCS values were determined for symmetrically branched (open) and linear (filled) PES oligomers without (A) and with 0.5 vol% NBA added (B) to the sample (Figure 8). A distinction is made between CCS values derived from 1+ (black), 2+ (red), 3+ (blue), and 4+ (green) ions. When no NBA is used, CCS values can be assigned up to d.p. 24; however, distinction between branched and linear chains is only possible up to d.p. 17. At higher d.p. values, the IM bands overlap too strongly to confidently assign CCS values to linear or symmetrically branched structures. Furthermore, the number of observed 3+ species is limited and 4+ ions are not detected. When NBA is added to the sample solution, the CCS for PES chains up to d.p. 29 could be confidently determined. Moreover, 3+ and 4+ ions are more abundant, which allows for structural assignment up to d.p. 29. The extra charging by sodium ions also highlights the difference in observable CCS values (ΔCCS) of the branched PES oligomers compared to the linear ones. This difference is indeed larger for higher charges. Notably, the observed CCS

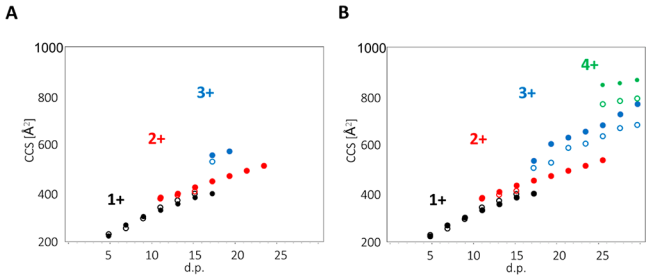


**Figure 8.** CCS values as a function of the d.p. for symmetrically branched (open circles) and linear (filled circles) oligomers without (A) and with 0.5 vol% NBA added (B) to sample 2 in 50/50 THF/water containing 100 mM NaI. A distinction is made between CCS values derived from 1+ (black), 2+ (red), 3+ (blue), and 4+ (green) charged ions.

value for a given d.p. increases with the number of charges on the oligomer, as is particularly apparent for d.p. 17. The increase is caused by the relative contribution of the sodium ion to the overall size of the oligomer as well as by the chain elongation induced by electrostatic repulsion between the adduct ions. This allows discrimination between linear and branched structures at higher d.p. values.

## CONCLUSION

The feasibility of TIMS for the separation of isomeric PES oligomers was assessed. DI-ESI-IMS of PES samples revealed signature masses of structures which contain a branching unit. As verified by LC-TIMS-MS/MS, the exact structures for small molecules could be assigned to the observed mobility bands by using ESI-TIMS-MS/MS. This was accomplished by constructing EIMs of both the parent and fragment ions revealing unique fragment ions for small linear polymeric species. In turn, this led to the assignment of branched species by means of fragmentation and the probability of occurring fragments. Larger polymers were initially not observed in the ion mobility dimension. To overcome this limitation, 0.5 vol% $m$-NBA was added to the sample solution to enhance ion charging (and reduce $1/K_0$). Employing pmCID to remove adducts post ion-mobility separation allowed partial structural assignment of larger isomeric species (up to 3000 Da). Overall, it is shown that the employed approach enables discrimination between branched and linear polymer architectures. The quantitation of the degree of branching remains challenging due to the large variety of structural isomers present. Future work encompasses creating an adequate and reliable quantitation tool for assessing the degree of branching with TIMS-MS. Another relevant study would be to further utilize online LC-timsTOF to enhance resolving constitutional isomers and stereoisomers, and to extend the polymer accessible mass range by postcolumn addition of $m$-NBA. Also, automated data analysis such as Kendrick mass defect tools that can deal with (polymer) timsTOF data would be beneficial and should be (further) developed.

## ASSOCIATED CONTENT

### Supporting Information

The Supporting Information is available free of charge at https://pubs.acs.org/doi/10.1021/jasms.1c00071.

Detailed description of NMR characterization, timsTOF schematic (Figure S1), repeatability of obtained mobility values (Figure S2; Table S1), polymer fragmentation



https://doi.org/10.1021/jasms.1c00071
J. Am. Soc. Mass Spectrom. 2021, 32, 1498−1507

behavior at varying eV (Figure S3), LC-UV-TIMS-MS(/MS) of polyester (Figure S4), factor of average signal increase by addition of *m*-NBA to the sample solutions (Figure S5), approach for structurally elucidating larger polymers using DI-ESI-TIMS-pmCID-MS/MS (Figure S6), and visualization of the structural assignment approach based on fragment EIMs (Figure S7) (PDF)

## AUTHOR INFORMATION


### Corresponding Author

**Rob Haselberg** − *Division of BioAnalytical Chemistry, Amsterdam Institute of Molecular and Life Sciences (AIMMS), Vrije Universiteit Amsterdam, 1081 HV Amsterdam, The Netherlands; Centre for Analytical Sciences Amsterdam (CASA), 1098 XH Amsterdam, The Netherlands;* orcid.org/0000-0003-1892-1724; Email: r.haselberg@vu.nl

### Authors

**Robert L. C. Voeten** − *Division of BioAnalytical Chemistry, Amsterdam Institute of Molecular and Life Sciences (AIMMS), Vrije Universiteit Amsterdam, 1081 HV Amsterdam, The Netherlands; TI-COAST, 1098 XH Amsterdam, The Netherlands; Centre for Analytical Sciences Amsterdam (CASA), 1098 XH Amsterdam, The Netherlands;* orcid.org/0000-0001-9054-4615

**Bram van de Put** − *TI-COAST, 1098 XH Amsterdam, The Netherlands; Centre for Analytical Sciences Amsterdam (CASA), 1098 XH Amsterdam, The Netherlands*

**Jan Jordens** − *DSM Materials Science Center, 6167 MD Geleen, The Netherlands*

**Ynze Mengerink** − *DSM Materials Science Center, 6167 MD Geleen, The Netherlands*

**Ron A. H. Peters** − *Centre for Analytical Sciences Amsterdam (CASA), 1098 XH Amsterdam, The Netherlands; DSM Resins & Functional Materials, Analytical Technology Centre, 5145 PE Waalwijk, The Netherlands; HIMS-Analytical Chemistry Group, University of Amsterdam, 1098 XH Amsterdam, The Netherlands*

**Govert W. Somsen** − *Division of BioAnalytical Chemistry, Amsterdam Institute of Molecular and Life Sciences (AIMMS), Vrije Universiteit Amsterdam, 1081 HV Amsterdam, The Netherlands; Centre for Analytical Sciences Amsterdam (CASA), 1098 XH Amsterdam, The Netherlands;* orcid.org/0000-0003-4200-2015

Complete contact information is available at: https://pubs.acs.org/10.1021/jasms.1c00071


### Notes

The authors declare no competing financial interest.

## ACKNOWLEDGMENTS

R.L.C.V. acknowledges the HOSAna Project, which is funded by The Dutch Research Council (NWO) in the framework of the Programmatic Technology Area PTA-COAST4 of the Fund New Chemical Innovations (project no. 053.21.117). We would like to acknowledge Dr. Paul Buijsen (DRF, Zwolle) who prepared and provided the studied polyester samples.

## REFERENCES


(1) Vanden Poel, G.; Istrate, D.; Mathot, V.; Schick, C.; Mathot, V. Full-Temperature-Range Crystallization Rates of Polyamides by Fast Scanning Calorimetry as Key to Processing. *Fast Scanning Calorimetry* **2016**, 611−632.

(2) Papageorgiou, G. Z.; Papageorgiou, D. G.; Tsanaktsis, V.; Bikiaris, D. N. Synthesis of the Bio-Based Polyester Poly(Propylene 2,5-Furan Dicarboxylate). Comparison of Thermal Behavior and Solid State Structure with Its Terephthalate and Naphthalate Homologues. *Polymer* **2015**, *62*, 28−38.

(3) Saba, N.; Jawaid, M.; Alothman, O. Y.; Paridah, M. T. A Review on Dynamic Mechanical Properties of Natural Fibre Reinforced Polymer Composites. *Constr. Build. Mater.* **2016**, *106*, 149−159.

(4) Essabir, H.; Bensalah, M. O.; Rodrigue, D.; Bouhfid, R.; Qaiss, A. Structural, Mechanical and Thermal Properties of Bio-Based Hybrid Composites from Waste Coir Residues: Fibers and Shell Particles. *Mech. Mater.* **2016**, *93*, 134−144.

(5) Lei, T.; Wang, J.-Y.; Pei, J. Design, Synthesis, and Structure-Property Relationships of Isoindigo-Based Conjugated Polymers. *Acc. Chem. Res.* **2014**, *47* (4), 1117−1126.

(6) Zhu, X.; Zhou, Y.; Yan, D. Influence of Branching Architecture on Polymer Properties. *J. Polym. Sci., Part B: Polym. Phys.* **2011**, *49* (18), 1277−1286.

(7) Crotty, S.; Gerişlioğlu, S.; Endres, K. J.; Wesdemiotis, C.; Schubert, U. S. Polymer Architectures via Mass Spectrometry and Hyphenated Techniques: A Review. *Anal. Chim. Acta* **2016**, *932*, 1−21.

(8) Vilaplana, F.; Gilbert, R. G. Characterization of Branched Polysaccharides Using Multiple-Detection Size Separation Techniques. *J. Sep. Sci.* **2010**, *33* (22), 3537−3554.

(9) Liu, P.; Liu, W.; Wang, W.-J.; Li, B.-G.; Zhu, S. A Comprehensive Review on Controlled Synthesis of Long-Chain Branched Polyolefins: Part 3, Characterization of Long-Chain Branched Polymers. *Macromol. React. Eng.* **2017**, *11* (1), 1600012.

(10) Wesdemiotis, C. Multidimensional Mass Spectrometry of Synthetic Polymers and Advanced Materials. *Angew. Chem., Int. Ed.* **2017**, *56* (6), 1452−1464.

(11) Eselem Bungu, P. S.; Pasch, H. Comprehensive Analysis of Branched Polyethylene: The Multiple Preparative Fractionation Concept. *Polym. Chem.* **2017**, *8* (31), 4565−4575.

(12) Gaborieau, M.; Castignolles, P. Size-Exclusion Chromatography (SEC) of Branched Polymers and Polysaccharides. *Anal. Bioanal. Chem.* **2011**, *399* (4), 1413−1423.

(13) Maniego, A. R.; Sutton, A. T.; Gaborieau, M.; Castignolles, P. Assessment of the Branching Quantification in Poly(Acrylic Acid): Is It as Easy as It Seems? *Macromolecules* **2017**, *50* (22), 9032−9041.

(14) Lena, J.-B.; Goroncy, A. K.; Thevarajah, J. J.; Maniego, A. R.; Russell, G. T.; Castignolles, P.; Gaborieau, M. Effect of Transfer Agent, Temperature and Initial Monomer Concentration on Branching in Poly(Acrylic Acid): A Study by 13C NMR Spectroscopy and Capillary Electrophoresis. *Polymer* **2017**, *114*, 209−220.

(15) Cook, A. B.; Barbey, R.; Burns, J. A.; Perrier, S. Hyperbranched Polymers with High Degrees of Branching and Low Dispersity Values: Pushing the Limits of Thiol-Yne Chemistry. *Macromolecules* **2016**, *49* (4), 1296−1304.

(16) Hawker, C. J.; Lee, R.; Frechet, J. M. J. One-Step Synthesis of Hyperbranched Dendritic Polyesters. *J. Am. Chem. Soc.* **1991**, *113* (12), 4583−4588.

(17) Sheveleva, N. N.; Markelov, D. A.; Vovk, M. A.; Mikhailova, M. E.; Tarasenko, I. I.; Neelov, I. M.; Lähderanta, E. NMR Studies of Excluded Volume Interactions in Peptide Dendrimers. *Sci. Rep.* **2018**, *8* (1), 8916.

(18) Thevarajah, J. J.; Sutton, A. T.; Maniego, A. R.; Whitty, E. G.; Harrisson, S.; Cottet, H.; Castignolles, P.; Gaborieau, M. Quantifying the Heterogeneity of Chemical Structures in Complex Charged Polymers through the Dispersity of Their Distributions of Electrophoretic Mobilities or of Compositions. *Anal. Chem.* **2016**, *88* (3), 1674−1681.

(19) Cottet, H.; Gareil, P.; Theodoly, O.; Williams, C. E. A Semi-Empirical Approach to the Modeling of the Electrophoretic Mobility in Free Solution: Application to Polystyrenesulfonates of Various Sulfonation Rates. *Electrophoresis* **2000**, *21* (17), 3529−3540.

(20) Nouri, S.; Dubois, C.; Lafleur, P. G. Homocrystal and Stereocomplex Formation Behavior of Polylactides with Different Branched Structures. *Polymer* **2015**, *67*, 227−239.
(21) Li, H.; Rojas, G.; Wagener, K. B. Precision Long-Chain Branched Polyethylene via Acyclic Diene Metathesis Polymerization. *ACS Macro Lett.* **2015**, *4* (11), 1225−1228.
(22) Chen, H.; Kong, J. Hyperbranched Polymers from A2 + B3 Strategy: Recent Advances in Description and Control of Fine Topology. *Polym. Chem.* **2016**, *7* (22), 3643−3663.
(23) Svedlund, F. L.; Altiok, E. I.; Healy, K. E. Branching Analysis of Multivalent Conjugates Using Size Exclusion Chromatography-Multiangle Light Scattering. *Biomacromolecules* **2016**, *17* (10), 3162−3171.
(24) Al Samman, M.; Radke, W.; Khalyavina, A.; Lederer, A. Retention Behavior of Linear, Branched, and Hyperbranched Polyesters in Interaction Liquid Chromatography. *Macromolecules* **2010**, *43* (7), 3215−3220.
(25) Ahn, S.; Lee, H.; Lee, S.; Chang, T. Characterization of Branched Polymers by Comprehensive Two-Dimensional Liquid Chromatography with Triple Detection. *Macromolecules* **2012**, *45* (8), 3550−3556.
(26) Clementi, L. A.; Vega, J. R.; Meira, G. R. Randomly-Branched Polymers by Size Exclusion Chromatography with Triple Detection: Computer Simulation Study for Estimating Errors in the Distribution of Molar Mass and Branching Degree. *Macromol. Theory Simul.* **2014**, *23* (2), 90−100.
(27) Pathaweeisariyakul, T.; Narkchamnan, K.; Thitisak, B.; Rungswang, W.; Yau, W. W. An Alternative Method for Long Chain Branching Determination by Triple-Detector Gel Permeation Chromatography. *Polymer* **2016**, *107*, 122−129.
(28) Thevarajah, J. J.; Gaborieau, M.; Castignolles, P. Separation and Characterization of Synthetic Polyelectrolytes and Polysaccharides with Capillary Electrophoresis. *Adv. Chem.* **2014**, *2014*, 798503.
(29) Wittenberg, N. F. G.; Preusser, C.; Kattner, H.; Stach, M.; Lacík, I.; Hutchinson, R. A.; Buback, M. Modeling Acrylic Acid Radical Polymerization in Aqueous Solution. *Macromol. React. Eng.* **2016**, *10* (2), 95−107.
(30) Hamzehlou, S.; Ballard, N.; Reyes, Y.; Aguirre, A.; Asua, J. M.; Leiza, J. R. Analyzing the Discrepancies in the Activation Energies of the Backbiting and $\beta$-Scission Reactions in the Radical Polymerization of n-Butyl Acrylate. *Polym. Chem.* **2016**, *7* (11), 2069−2077.
(31) Jung, M.; Lee, Y.; Kwak, S.; Park, H.; Kim, B.; Kim, S.; Lee, K. H.; Cho, H. S.; Hwang, K. Y. Analysis of Chain Branch of Polyolefins by a New Proton NMR Approach. *Anal. Chem.* **2016**, *88* (3), 1516−1520.
(32) Fischer, A. M.; Schüll, C.; Frey, H. Hyperbranched Poly(Glycolide) Copolymers with Glycerol Branching Points via Ring-Opening Copolymerization. *Polymer* **2015**, *72*, 436−446.
(33) Al Samman, M.; Radke, W. Two-Dimensional Chromatographic Separation of Branched Polyesters According to Degree of Branching and Molar Mass. *Polymer* **2016**, *99*, 734−740.
(34) Edam, R.; Meunier, D. M.; Mes, E. P. C.; Van Damme, F. A.; Schoenmakers, P. J. Branched-Polymer Separations Using Comprehensive Two-Dimensional Molecular-Topology Fractionation × size-Exclusion Chromatography. *J. Chromatogr. A* **2008**, *1201* (2), 208−214.
(35) Schoenmakers, P.; Aarnoutse, P. Multi-Dimensional Separations of Polymers. *Anal. Chem.* **2014**, *86* (13), 6172−6179.
(36) Cheruthazhekatt, S.; Pijpers, T. F. J.; Harding, G. W.; Mathot, V. B. F.; Pasch, H. Multidimensional Analysis of the Complex Composition of Impact Polypropylene Copolymers: Combination of TREF, SEC-FTIR-HPer DSC, and High Temperature 2D-LC. *Macromolecules* **2012**, *45* (4), 2025−2034.
(37) Haler, J. R. N.; Far, J.; Aqil, A.; Claereboudt, J.; Tomczyk, N.; Giles, K.; Jérôme, C.; De Pauw, E. Multiple Gas-Phase Conformations of a Synthetic Linear Poly(Acrylamide) Polymer Observed Using Ion Mobility-Mass Spectrometry. *J. Am. Soc. Mass Spectrom.* **2017**, *28* (11), 2492−2499.
(38) Duez, Q.; Josse, T.; Lemaur, V.; Chirot, F.; Choi, C. M.; Dubois, P.; Dugourd, P.; Cornil, J.; Gerbaux, P.; De Winter, J. Correlation between the Shape of the Ion Mobility Signals and the Stepwise Folding Process of Polylactide Ions. *J. Mass Spectrom.* **2017**, *52* (3), 133−138.
(39) Alalwiat, A.; Tang, W.; Gerişlioğlu, S.; Becker, M. L.; Wesdemiotis, C. Mass Spectrometry and Ion Mobility Characterization of Bioactive Peptide-Synthetic Polymer Conjugates. *Anal. Chem.* **2017**, *89* (2), 1170−1177.
(40) Shi, C.; Gerişlioğlu, S.; Wesdemiotis, C. Ultrahigh Performance Liquid Chromatography Interfaced with Mass Spectrometry and Orthogonal Ion Mobility Separation for the Microstructure Characterization of Amphiphilic Block Copolymers. *Chromatographia* **2016**, *79* (15), 961−969.
(41) Ridgeway, M. E.; Lubeck, M.; Jordens, J.; Mann, M.; Park, M. A. Trapped Ion Mobility Spectrometry: A Short Review. *Int. J. Mass Spectrom.* **2018**, *425*, 22−35.
(42) Gabelica, V.; Shvartsburg, A. A.; Afonso, C.; Barran, P.; Benesch, J. L. P.; Bleiholder, C.; Bowers, M. T.; Bilbao, A.; Bush, M. F.; Campbell, J. L.; Campuzano, I. D. G.; Causon, T.; Clowers, B. H.; Creaser, C. S.; De Pauw, E.; Far, J.; Fernandez-Lima, F.; Fjeldsted, J. C.; Giles, K.; Groessl, M.; Hogan, C. J., Jr.; Hann, S.; Kim, H. I.; Kurulugama, R. T.; May, J. C.; McLean, J. A.; Pagel, K.; Richardson, K.; Ridgeway, M. E.; Rosu, F.; Sobott, F.; Thalassinos, K.; Valentine, S. J.; Wyttenbach, T. Recommendations for Reporting Ion Mobility Mass Spectrometry Measurements. *Mass Spectrom. Rev.* **2019**, *38* (3), 291−320.
(43) Silveira, J. A.; Ridgeway, M. E.; Park, M. A. High Resolution Trapped Ion Mobility Spectrometery of Peptides. *Anal. Chem.* **2014**, *86* (12), 5624−5627.
(44) Morsa, D.; Defize, T.; Dehareng, D.; Jérôme, C.; De Pauw, E. Polymer Topology Revealed by Ion Mobility Coupled with Mass Spectrometry. *Anal. Chem.* **2014**, *86* (19), 9693−9700.
(45) Liu, X.; Cool, L. R.; Lin, K.; Kasko, A. M.; Wesdemiotis, C. Tandem Mass Spectrometry and Ion Mobility Mass Spectrometry for the Analysis of Molecular Sequence and Architecture of Hyperbranched Glycopolymers. *Analyst* **2015**, *140* (4), 1182−1191.
(46) Foley, C. D.; Zhang, B.; Alb, A. M.; Trimpin, S.; Grayson, S. M. Use of Ion Mobility Spectrometry-Mass Spectrometry to Elucidate Architectural Dispersity within Star Polymers. *ACS Macro Lett.* **2015**, *4* (7), 778−782.
(47) Charles, L.; Chendo, C.; Poyer, S. Ion Mobility Spectrometry - Mass Spectrometry Coupling for Synthetic Polymers. *Rapid Commun. Mass Spectrom.* **2020**, *34*, No. e8624.
(48) Gies, A. P.; Kliman, M.; McLean, J. A.; Hercules, D. M. Characterization of Branching in Aramid Polymers Studied by MALDI-Ion Mobility/Mass Spectrometry. *Macromolecules* **2008**, *41* (22), 8299−8301.
(49) Austin, C. A.; Inutan, E. D.; Bohrer, B. C.; Li, J.; Fischer, J. L.; Wijerathne, K.; Foley, C. D.; Lietz, C. B.; Woodall, D. W.; Imperial, L. F.; Clemmer, D. E.; Trimpin, S.; Larsen, B. S. Resolving Isomers of Star-Branched Poly(Ethylene Glycols) by IMS-MS Using Multiply Charged Ions. *J. Am. Soc. Mass Spectrom.* **2021**, *32*, 21.
(50) Wesdemiotis, C.; Solak, N.; Polce, M. J.; Dabney, D. E.; Chaicharoen, K.; Katzenmeyer, B. C. Fragmentation Pathways of Polymer Ions. *Mass Spectrom. Rev.* **2011**, *30* (4), 523−559.
(51) Ludwig, M.; Broeckling, C. D.; Dorrestein, P.; Dührkop, K.; Schymanski, E.; Boecker, S.; Nothias, L.-F. Mining the NIST Mass Spectral Library Reveals the Extent of Sodium Assisted Inductive Cleavage in Collision-Induced Fragmentation. *chemrxiv.org* **2020**, DOI: 10.26434/chemrxiv.12114987.v1.
(52) Miladinović, S. M.; Fornelli, L.; Lu, Y.; Piech, K. M.; Girault, H. H.; Tsybin, Y. O. In-Spray Supercharging of Peptides and Proteins in Electrospray Ionization Mass Spectrometry. *Anal. Chem.* **2012**, *84* (11), 4647−4651.
(53) Iavarone, A. T.; Jurchen, J. C.; Williams, E. R. Supercharged Protein and Peptide Ions Formed by Electrospray Ionization. *Anal. Chem.* **2001**, *73* (7), 1455−1460.

(54) Ogorzalek Loo, R. R.; Lakshmanan, R.; Loo, J. A. What Protein Charging (and Supercharging) Reveal about the Mechanism of Electrospray Ionization. *J. Am. Soc. Mass Spectrom.* **2014**, *25* (10), 1675−1693.
(55) Steinkoenig, J.; Cecchini, M. M.; Reale, S.; Goldmann, A. S.; Barner-Kowollik, C. Supercharging Synthetic Polymers: Mass Spectrometric Access to Nonpolar Synthetic Polymers. *Macromolecules* **2017**, *50* (20), 8033−8041.



https://doi.org/10.1021/jasms.1c00071
*J. Am. Soc. Mass Spectrom.* 2021, 32, 1498−1507